A New Control Strategy for the Improvement of Contact Rendering with Encounter-type Haptic Displays

Oscar De La Cruz Fierro[1,2,3,4], Wael Bachta[2,3,4], Florian Gosselin[1] and Guillaume Morel[2,3,4]
[1]*Interactive Robotics Laboratory, CEA, LIST, F-91190, Gif-sur-Yvette, France*
[2]*Institut des Systèmes Intelligents et de Robotique, Sorbonne Universités, UPMC Univ. Paris 06, F-75005, Paris, France*
[3]*Institut des Systèmes Intelligents et de Robotique, CNRS, UMR 7222, F-75005, Paris, France*
[4]*Institut des Systèmes Intelligents et de Robotique, Equipe Agathe, INSERM, ERL U1150, F-75005, Paris, France*

Keywords: Robot Control, Haptic Interface, Encounter-type Haptic Display (ETHD).

Abstract: Encounter-type haptic interfaces are used to interact physically with virtual environments. They allow controlling the position of an avatar in the simulation while perceiving the forces applied on it when it interacts with the surrounding objects. Contrary to usual force feedback devices, the interface tracks the real user's finger without touching it when the user's finger avatar moves in free space. Only when a contact occurs in the virtual environment, the interface comes in contact with the user to display the mechanical properties of the encountered objects. This way, the device's behaviour is more natural as simulated contacts really occur in the real world. Existing control laws for such devices exhibit however limitations, especially when contacts occur at high speed. In such cases, the device tends to bounce against the user's finger, which decreases the realism of the interaction. In this paper, we propose a new control strategy where the interface is first stabilized against the obstacles before the user touches its end-effector. This way, contacts appear more natural, even at high speeds, as confirmed by preliminary user-tests made with an existing 2 DoF encounter type haptic interface at different speeds with the state of the art control law and the novel approach we propose here.

1 INTRODUCTION

Haptic interfaces allow motion interactions with virtual or remote environments with a reproduction of the sense of touch, using kinesthetic (force/position) and cutaneous (tactile) receptors (Hannaford and Okamura, 2008). We can distinguish four methods for creating haptic sensations artificially: vibrotactile devices, force-feedback systems (discussed in this paper), surface displays and distributed tactile displays (Hayward and Maclean, 2007).

Force-feedback systems are robotic mechanisms capable to measure the user's movements and deliver a force signal to the operator's hand, usually through a pen-like interface, a knob or a thimble (Campion, 2011). A non-exhaustive list of application cases are computer-aided design (Nahvi et al., 1998), maintenance and assembly tasks (McNeely et al., 1999), games (Martin and Hillier, 2009) and virtual reality task simulations (Sagardia et al., 2015) as well as teleoperation (Gosselin et al., 2005).

In an ideal force-feedback system, the user should be able to move in free space without feeling any force and the device should prevent him/her to move in the constraint direction if a stiff object is being touched. In the mentioned application contexts however, force-feedback interfaces usually require the user to be mechanically linked to them. This link has a non-negligible influence: the user experiences the friction, inertia and vibrations of the mechanical structure even when moving in free space, which reduces the realism of the interaction. In addition, the difference between free space and contact is less distinctively felt than in real world.

Encounter-Type Haptic Displays (ETHDs) propose, as a solution to this problem, to remove the mechanical link between the interface and the operator (McNeely, 1993), (Tachi et al., 1994). This principle allows a perfect transparency in free space motion as the user touches the haptic device, usually with the fingertip, only when a contact occurs in the virtual/remote environment (see Figure 1). (Yoshikawa and Nagura, 1997) and (Yoshikawa and Nagura, 1999) use for example a set of optical glass-fiber on-off sensors for measuring the position of the operator's finger, respectively in 2D space with a

Fierro, O., Bachta, W., Gosselin, F. and Morel, G.
A New Control Strategy for the Improvement of Contact Rendering with Encounter-type Haptic Displays.
DOI: 10.5220/0006474704710480
In *Proceedings of the 14th International Conference on Informatics in Control, Automation and Robotics (ICINCO 2017) - Volume 2*, pages 471-480
ISBN: Not Available

ring-like end-effector and in 3D space with a cap-like end-effector. The position of the finger is however only roughly estimated. In (Gonzalez et al., 2015a) a ring-like end-effector instrumented with infrared proximity sensors, mounted on a 2 Degrees of Freedom (DoF) interface, is used to reconstruct the shape of the finger and precisely estimate its position using distance measurements (Gonzalez et al., 2015b). We find as well hand exoskeletons (Nakagawara et al., 2005), (Fang et al., 2009) where the position of a thin reflecting plate, pushed by the nail, is recorded thanks to an optical sensor. Force felt between the plate and the finger is negligible.

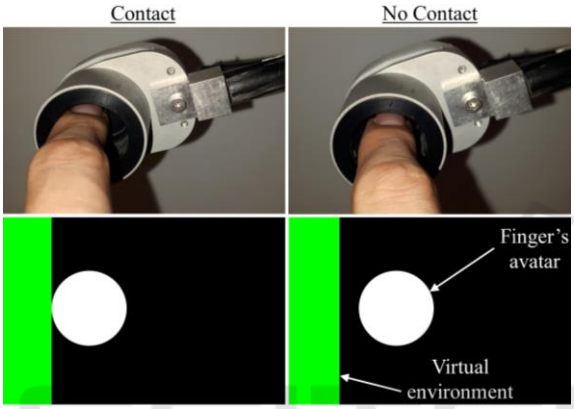

Figure 1: Encounter-type haptic display principle.

Special attention should be given to the control law that governs ETHDs, particularly to the transitions between free space and contact modes. As shown in (Gonzalez et al., 2015a), control strategies usually implemented on ETHDs rely on an abrupt transition between these two modes, potentially generating vibrations and non-realistic impact forces at that moment. To cope with this issue, (Gonzalez et al., 2015a) proposes a smooth transition-based control. This solution was implemented on a 2DoF ETHD. It proves stable and more realistic, especially when finger interactions occur at low speeds (≈0.2 m/s). However at higher speeds the problem is not completely tackled and the sensation felt may be non-realistic at the moment of contact.

In this paper, we propose a new control strategy aimed at allowing natural transitions between free space and contact modes, even at higher speeds (>0.2 m/s). It includes a bilateral damping allowing the stabilization of the robot's end-effector before application of force feedback. This comes at the price of a slight shift of the virtual wall, which remains however imperceptible for most users as proved by the results of our evaluations. The state of the art control law implemented in (Gonzalez et al., 2015a) is first briefly presented in section 2. The proposed upgraded control strategy is then explained in section 3. Section 4 presents the results of the experiments performed to validate the potential of our approach. Finally conclusions are given in section 5.

2 SMOOTH TRANSITION-BASED CONTROL

In free space, the ETHD should closely track the finger's position without touching it. When the user's avatar enters in contact with a virtual wall, the resulting contact force should be displayed to the user. A control law, which to our knowledge answers the most closely the aforementioned requirements, was proposed in (Gonzalez et al., 2015a) and implemented on a 2DoF ETHD. It will be briefly described in the following lines.

2.1 Control Algorithm for Finger Tracking in Free Space

We note here $\boldsymbol{\epsilon_X} = \boldsymbol{X_{f/0}} - \boldsymbol{X_{r/0}} = \boldsymbol{X_{f/r}}$ the position error between the ring center and the finger center (see Figure 2). Being small as close tracking of the finger is desired, it can be expressed in joint space:

$$\boldsymbol{\epsilon_q} = \mathbf{J}^{-1}(\boldsymbol{q}) \cdot \boldsymbol{\epsilon_X} \quad (1)$$

where $\boldsymbol{q} = [\,q_1 \quad q_2\,]^T$ are the joints positions and $\mathbf{J}(\boldsymbol{q})$ the robot's jacobian matrix expressed in its global reference frame $\boldsymbol{R_0}$.

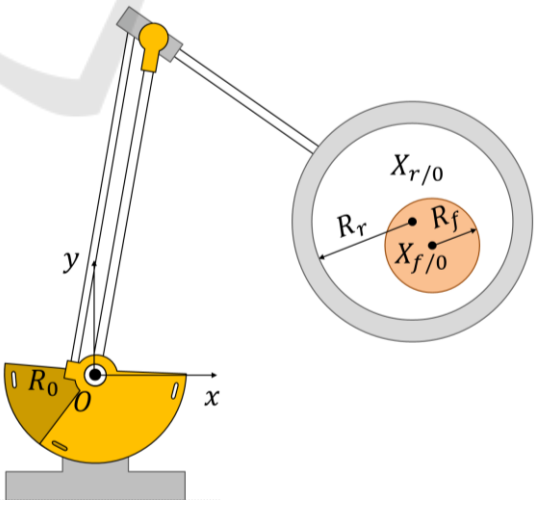

Figure 2: 2DoF ETHD with ring center $X_{r/0}$and finger center $X_{f/0}$(adapted from (Gonzalez, 2015)).

Error minimization is achieved with a Proportional Derivative controller, which provides the robot with a reference torque:

$$\boldsymbol{\tau_t} = \mathbf{Z_t} \cdot \boldsymbol{\epsilon_q} = (\mathbf{K_t} + \mathbf{B_t}s) \cdot \boldsymbol{\epsilon_q} \quad (2)$$

where $\mathbf{Z_t}$ is the equivalent impedance, $\mathbf{K_t}$ and $\mathbf{B_t}$ the proportional and derivative gains respectively. With this controller, a link equivalent to a spring and damper system is created between the centers of the user's finger and of the ring (see Figure 3).

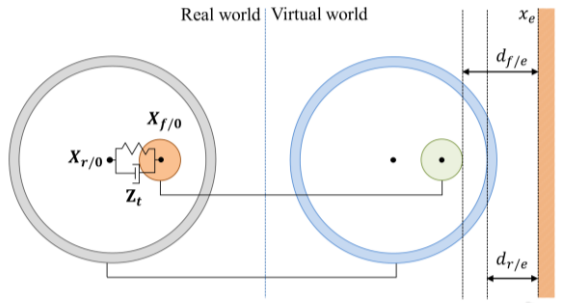

Figure 3: Spring damper coupling between the center of the finger $X_{f/0}$and the center of the ring $X_{r/0}$in free space.

2.2 Control Algorithm for Force Rendering at Contact

When a virtual object is encountered, the interface must render the corresponding interaction force $\mathbf{F_e}$, which is defined as an unilateral constraint. A viscoelastic compliant virtual environment without tangential friction is assumed and a modified Kelvin-Voigt model (Achhammer et al., 2010) is used to calculate the resulting interaction forces (see Eq. 3).

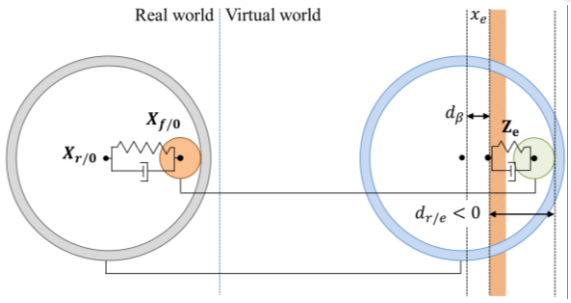

Figure 4: At contact the influence of the tracking force $\mathbf{F_t}$has been diminished by a factor $\beta$and a spring and damper coupling ($\mathbf{Z_e} = \mathbf{K_e} + \mathbf{B_e}s$) is created between the ring and the wall to render the interaction force $\mathbf{F_e}$.

Let $d_{r/e}$ be the distance between the ring's avatar inner circumference and the closest point of a virtual object, x_e the position of a vertical wall (see Figure 4), $\mathbf{n}$ a unitary vector normal to the surface of contact, $\dot{X}_{r/0}$ the speed of the ring along $\mathbf{n}$. The environment interaction force $\mathbf{F_e}$ can be expressed as follows:

$$\begin{cases} if\ d_{r/e} < 0\ \&\ \dot{X}_{r/0} > 0 & \mathbf{F_e} = d_{r/e}(\mathbf{K_e} + \mathbf{B_e}s)\mathbf{n} \\ if\ d_{r/e} < 0\ \&\ \dot{X}_{r/0} < 0 & \mathbf{F_e} = d_{r/e}\mathbf{K_e}\mathbf{n} \\ else & \mathbf{F_e} = 0 \end{cases} \quad (3)$$

The transition between free space and contact is achieved by reducing the influence of the tracking force $\mathbf{F_t}$ by a factor β nearby the obstacles, i.e. at a distance $d_{f/e} = d_\beta$ from the virtual object (VO) placed at position x_e. Equation 4 shows how β varies in function of $d_{f/e}$, the distance between the finger's avatar and the VO (see Figure 3). Factor β cannot be totally cancelled at the proximity of the wall as in this case the ring would not follow the finger when it moves away from it.

$$\begin{cases} if\ d_{f/e} > d_\beta & \beta = 1 \\ if\ d_{f/e} \in\ ]0; d_\beta] & \beta = \left(\frac{1-\beta_{min}}{d_\beta}\right) d_{f/e} + \beta_{min} \\ if\ d_{f/e} \leq 0 & \beta = \beta_{min} = 0.1 \end{cases} \quad (4)$$

Here $d_\beta = R_r - R_{f,max}$,with $R_{f,max}$ chosen so that $\forall\ R_f$, $R_{f,max} > R_f$. This way by the moment the user encounters the ring, the tracking effect is almost canceled and $\|\mathbf{F_e}\| \neq 0$. The updated Eq. (2) can now be expressed as:

$$\boldsymbol{\tau_t} = \beta \mathbf{Z_t} \boldsymbol{\epsilon_q} \quad (5)$$

While allowing a smooth transition between free space and contact, this algorithm presents in practice an undesired behaviour when impacting virtual objects at high speeds (> 0.2 m/s): oscillations appear when the ring encounters a virtual object and therefore an unnatural contact is perceived by the user when his/her finger encounters the ring. It may give the impression of touching a moving object instead of a static one as in the real life.

3 OFFSET TRANSITION-BASED CONTROL

When the user's finger encounters the ring, he/she should feel as touching a static object. The offset transition-based control introduced in this paper proposes therefore to first apply a dissipating force when the ring's avatar penetrates into the VO in order to stop it before displaying the VO properties $\mathbf{Z_e}$. Further details will be given below.

3.1 Virtual Environment Force Estimation and Rendering

In free space, the user can move the interface freely, i.e. no interaction force exists. When the ring's inner periphery penetrates in a virtual object, we propose to completely stop it before displaying the VO properties. Therefore a dissipating force is applied on the ring until the interface is static (in practice until $|\dot{X}_{r/0}| < v_{th}$, with v_{th} an experimentally tuned threshold introduced to cope with the speed signal's noise). When the mentioned condition is true, the VO properties ($\mathbf{K_e}$ and $\mathbf{B_e}$) are rendered to the user. The new virtual wall position x_ε is defined as the coordinate of the distal point on the inner periphery of the ring once it is static.

This algorithm was implemented using a Finite State Machine (FSM) as shown in Figure 5. The initial state is called transparent: in this mode only the tracking force acts on the ring and $\mathbf{F_e} = 0$. As soon as the interface approaches the VO and the inner periphery of the ring penetrates into it (i.e. $d_{r/e} < 0$), the braking state becomes active. The applied bilateral force $\mathbf{F_d}$ exerted on the ring is shown in equation 6 with $\mathbf{B_d}$ the dissipative gain.

$$\mathbf{F_d} = -\dot{X}_{r/0}\mathbf{B_d}\mathbf{n} \qquad (6)$$

When $|\dot{X}_{r/0}| < v_{th}$ the VO state becomes active. The speed threshold is fixed to $v_{th} \approx 0.020$ m/s, which in practice corresponds to a static interface with a finger inside the ring. In this state the VO properties are the same as implemented in the original control law.

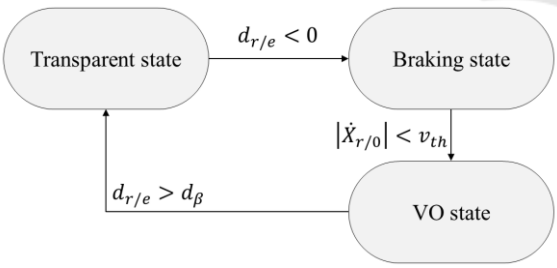

Figure 5: Finite State Machine governing the proposed control law.

Equation 7 defines $\mathbf{F_e}$ in reference to the new wall at position x_ε, where $d_{r/\varepsilon}$ is the distance between the inner ring periphery and it.

$$\begin{cases} if\ d_{r/\varepsilon} < 0\ \&\ \dot{X}_{r/0} > 0 & \mathbf{F_e} = d_{r/\varepsilon}(\mathbf{K_e} + \mathbf{B_e}s)\mathbf{n} \\ if\ d_{r/\varepsilon} < 0\ \&\ \dot{X}_{r/0} < 0 & \mathbf{F_e} = d_{r/\varepsilon}\mathbf{K_e}\mathbf{n} \\ else & \mathbf{F_e} = 0 \end{cases} \qquad (7)$$

3.2 Tracking Force

As previously explained, the influence of the tracking force must diminish when the ring touches the wall, however it must be strong enough for the interface to follow his/her finger when moving away from the VO. Also, it is important to have a continuous tracking force to ensure that the interface will behave correctly during transitions between free and contact modes. In the original control law $\mathbf{F_t}$ decreases by a factor β, which is function of $d_{f/e}$, to ensure its continuity (see section 2.2).

The control algorithm presented in section 3.1 requires a different strategy to make sure that the tracking force remains continue. β still varies in function of $d_{f/e}$ as in (4) but we make here $R_f = R_r$ so that the minimum value of $\mathbf{F_t}$ when the ring's avatar penetrates in the reference wall is ensured. Indeed, because of the tracking error, the finger's center position is always in advance to that of the ring when it is in movement. This means that if we consider a finger avatar the size of the ring, it will always penetrate first in the reference (x_e) or offset (x_ε) VO position. When the VO takes its new value at x_ε, the augmented finger's avatar is already penetrating into it. At this moment β varies in function of $d_{f/\varepsilon}$ to ensure the continuity of β and therefore that of $\mathbf{F_t}$. When moving away from the VO, the augmented finger avatar can be far enough from it in order too fully reactivate $\mathbf{Ft}$. When the ring comes back in transparent state, this is when $d_{r/e} > d_\beta$, we do β to vary in function of $d_{f/e}$ again. This way the continuity of the tracking force is ensured during all state transitions (see Figure 6).

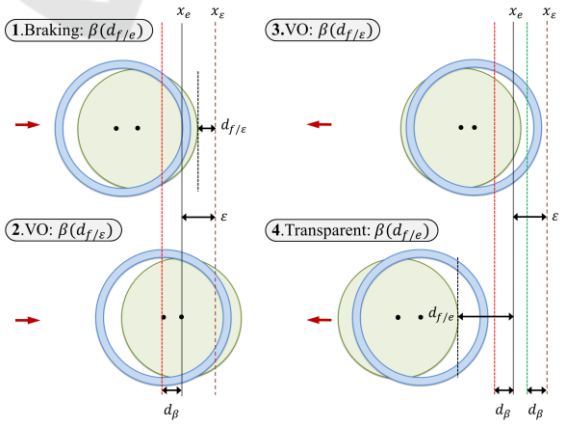

Figure 6: Variation of $\beta$for a typical encounter and related active state at each stage. εrepresents the wall offset.

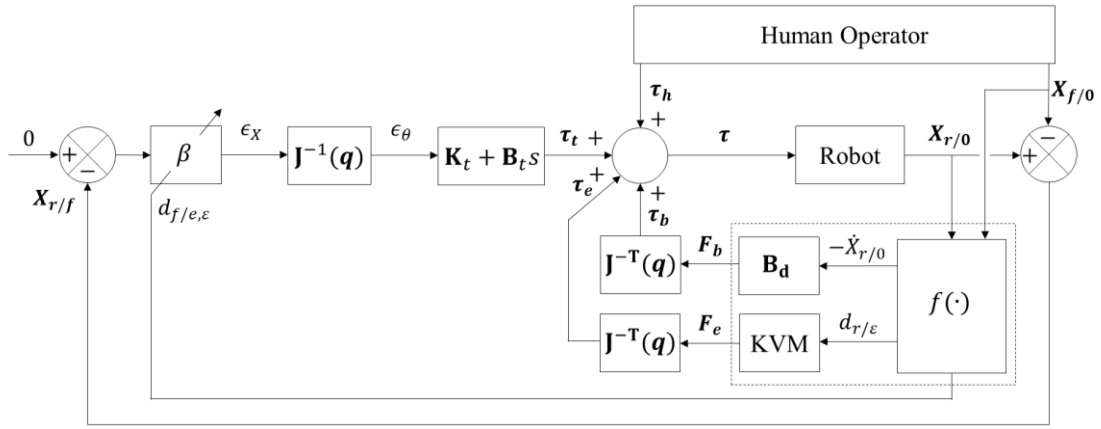

Figure 7: Offset transition-based control. KVM:interaction force. $f(\cdot)$: estimation of the robot's end-effector speed $\dot{X}_{r/0}$with negative sign and of the distance $d_{f/\varepsilon}$.

As we can observe in equation 8, the distance d_β is also valid when the VO state is active. Here $d_{f/e,\varepsilon}$ means that β will be function either of $d_{f/e}$ or $d_{f/\varepsilon}$, according to the active state (see Figure 6)**.** The control explained in sections 3.1 and 3.2 is resumed in the control block diagram from Figure 7.

$$\begin{cases} if\ d_{f/e,\varepsilon} > d_\beta & \beta = 1 \\ if\ d_{f/e,\varepsilon} \in]0; d_\beta]\ \beta = \left(\frac{1-\beta_{min}}{d_\beta}\right) d_{f/e,\varepsilon} + \beta_{min} \\ if\ d_{f/e,\varepsilon} \leq 0 & \beta = \beta_{min} = 0.1 \end{cases} \quad (8)$$

4 EXPERIMENTS AND RESULTS

To validate the benefits of the new approach, called VO-B (Virtual Object B) in the following, we have compared its performances with that of the original control law, called VO-A (Virtual Object A).

4.1 Experimental Setup

The robot used for these experiments is an optimized version of a 2D substructure of a parallel 6DoF haptic interface developed at CEA, LIST for tele-surgery (Gosselin et al., 2005). This 2 DoF robot is composed of two links 0.25 m long each (see Figure 8). Its workspace lies in a vertical plane. Actuation is provided by two Maxon RE-35 DC motors and cable capstan reducers, allowing a particularly transparent behaviour. 1000ppt encoders are used for position sensing and counterweights mounted on each axis allow gravity compensation. The 2D ring-shaped encounter-type end effector has an inner diameter of 24 mm, sufficient to track a finger at medium speeds. Sixteen Vishay VCNL4000 infrared proximity sensors distributed over the inner side of the ring make possible the estimation of a finger's center position at a rate of 300 Hz with a ± 0.3 mm precision.

Figure 8: 2DoF ETHD.

ATMega328P microcontrollers retrieve and send proximity sensor measurements to the haptic interface controller trough a fast serial bus at a rate of 400 kbps. Estimation of the finger's location is computed as the center of the polygon obtained from the measurement. The controller is composed of a PC104 computer running Xenomai realtime operating system and a servo-drive controlling both motors. A telerobotics library (Gicquel et al., 2001) acquires the state of the robot, computes the finger's position and sends the reference torques to the servo-drive at a rate of 1 KHz. Rate mismatch between the control loop (1 KHz) and the estimation of the finger's center (300 Hz) is handled by a Kalman filter committed to extrapolating the finger's position.

4.2 Practical Comparison between Smooth Transition-based and Offset Transition-based Control

In order to compare algorithms VO-A and VO-B, we made a typical encounter with a vertical virtual wall. We asked therefore a participant to move the ETHD horizontally from the right to the left with his index finger until he taps on a vertical wall located a few centimetres on the left of the initial position. In order to ensure an as natural as possible contact, we asked the user to keep his index finger straight and perpendicular to the working plane of the robot, with the pulp oriented to the left. These experiments were made both at low speed, where the existing control law is assumed to work properly, and at higher speeds, for which the device's behaviour becomes unnatural. The participant had a sufficient time to understand these instructions and familiarize with the interface. We checked both visually during the experiments and during data post-processing that the gesture was performed properly. It is worth noting that in practice, due to the limited dynamics of the robot, the user enters in contact with the ring before he encounters the wall for speeds higher than 0.5 m/s. We chose therefore 0.4 m/s as high speed. A value of 0.2 m/s was chosen for the low speed so as to remain significantly lower than the high speed.

The robot's gains were defined experimentally, so as to be the highest possible while remaining stable. Their values in free space and during contacts are given in equations 9 and 10 respectively. We use the same gains $\mathbf{K_t}$, $\mathbf{B_t}$ and $\mathbf{K_e}$, $\mathbf{B_e}$ in both conditions VO-A and VO-B. The dissipative gain $\mathbf{B_d}$ is defined in equation 11. A high value is chosen in order to stop the interface as fast as possible (in practice in less than 20ms, see Table 1). With these values, no instabilities were observed in practice.

$$\boldsymbol{K_t} = \begin{bmatrix} 40 & 0 \\ 0 & 40 \end{bmatrix} \text{Nm/rad} \quad \boldsymbol{B_t} = \begin{bmatrix} 1 & 0 \\ 0 & 1 \end{bmatrix} \text{Nms/rad} \qquad (9)$$

$$\mathbf{K_e} = \begin{bmatrix} 2500 & 0 \\ 0 & 2500 \end{bmatrix} \text{N/m} \quad \mathbf{B_e} = \begin{bmatrix} 45 & 0 \\ 0 & 45 \end{bmatrix} \text{Ns/m} \qquad (10)$$

$$\mathbf{B_d} = \begin{bmatrix} 100 & 0 \\ 0 & 100 \end{bmatrix} \text{Ns/m} \qquad (11)$$

In both cases, we denote $t_{r/vo}$ the instant of time at which the ring's inner periphery encounters the object's reference constraint, $to_{f/r}$ the instant of time when the user's finger contacts the ring, d_{max} the amplitude of the very first rebound of the end-effector at contact and x_e as the reference constraint. In condition VO-B, x_ε represent the modified constraint which is actually x_e plus the offset ε. Regarding speeds, we denote $v_r(t_{r/vo})$ the speed of the ring's center when it encounters the reference wall x_ε, $v_r(to_{f/r})$ its speed when it encounters the user's finger and $v_{r_{min}}(> to_{f/r})$ its minimal speed just after the finger encountered the ring.

4.2.1 Low Speed Case

The results obtained at low speed are given in Figures 9 and 10. No significant discrepancy can be observed between VO-A and VO-B. Both d_{max} and $v_r(to_{f/r})$ look similar. Only the speed $v_{r_{min}}(> to_{f/r})$, i.e. the rebound speed, is slightly smaller in condition VO-B. As a whole, the behaviour of both control laws is very similar. This is not a surprise as VO-A has already good performances at low speeds.

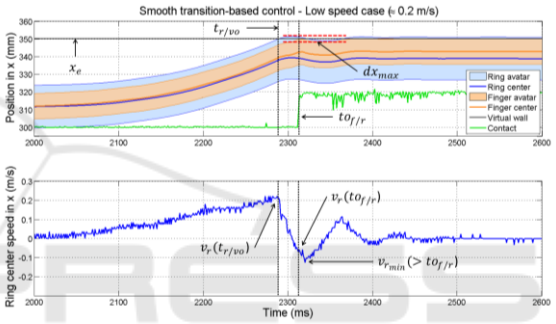

Figure 9: Typical encounter with a vertical virtual wall at a low speed in condition VO-A.

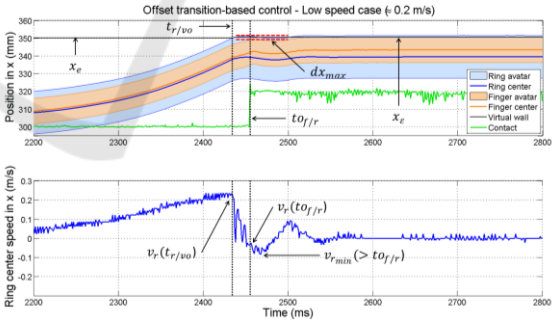

Figure 10: Typical encounter with a vertical virtual wall at a low speed in condition VO-B.

4.2.2 High Speed Case

A clear difference between VO-A and VO-B can be observed in this case (see Figure 11 and Figure 12), considering both d_{max}, which is smaller for VO-B (observable oscillations appear in VO-A) and $v_r(to_{f/r})$, which is closer to zero in VO-B, indicating that in this case the ring is quasi-static, as expected

(the observed oscillations prove on the contrary that this is not the case in condition VO-A).

Rebound speed $v_{r_{min}}(> to_{f/r})$ is also higher in VO-A than in VO-B. These observations lead us to make the hypothesis that with the new algorithm proposed in this article the sensation felt by the user will be more realistic since $v_r(to_{f/r})$ and $v_{r_{min}}(> to_{f/r})$ tend to be smaller at high speeds than in condition VO-A.

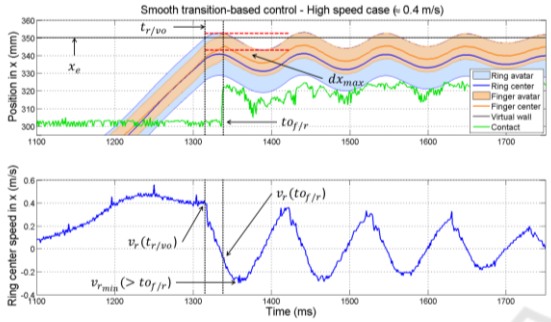

Figure 11: Typical encounter with a vertical virtual wall at a high speed in condition VO-A.

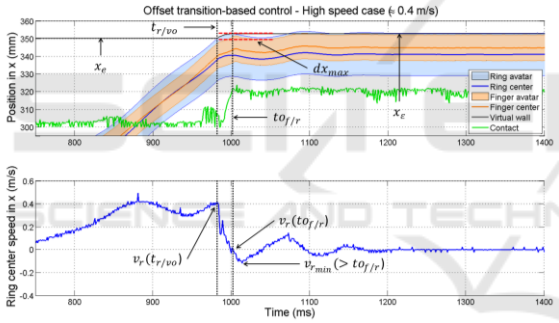

Figure 12: Typical encounter with a vertical virtual wall at a high speed in condition VO-B.

4.3 User Tests

According to (Samur, 2012), many factor studies can be used to assess the benefits of haptic feedback on sensory-motor tasks: peg-in-hole, tapping, targeting, etc. In the present work, we are more particularly interested in comparing how much the interface stabilizes when contacting a virtual object and how natural the contact is perceived by the user. As a consequence, we chose a tapping test to qualify the behaviour of the interface at both low and high speeds using VO-A and VO-B. The metrics introduced in section 4.2 will guide our analysis. The perception of the interaction was also evaluated through a survey.

4.3.1 Methodology

Four right-handed volunteers (3 men, 1 woman), aged 23-31, were invited to perform the tapping test. A printed document describing the experiment was given to each participant and he/she was asked to sign a letter of consent. The experiment was performed in an isolated room. The participant was standing, facing a screen and wearing an anti-noise helmet. The haptic interface was placed on a table so that his/her right index finger can be placed comfortably inside the end effector and so that a horizontal movement to the left can be performed easily.

A devoted graphical user interface (GUI) was developed for this experiment. It displays a 2D virtual environment in which the free space appears as a black vertical rectangle, surrounded by a thick green contour representing four virtual walls. The user is asked to tap on the left wall at low and high speeds, as previously defined in section 4.2, in conditions VO-A and VO-B. A white circle represents his/her finger and a vertical line indicates where to start before each tap (see Figure 13). In both conditions the finger's avatar is stopped against the wall, even if the robot, hidden by a vertical barrier, goes further, in order to avoid the influence of visual cues.

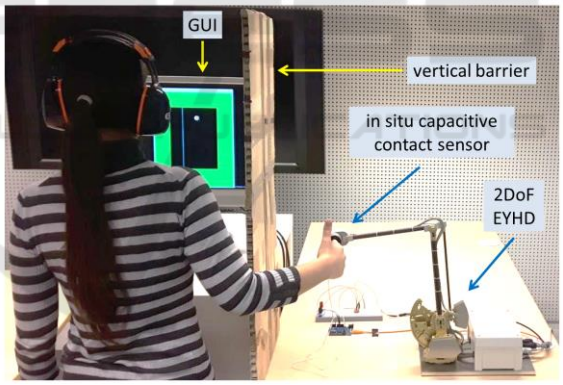

Figure 13: Setup of the experiment.

Low speed tests were always performed first, the order of presentation of each case being alternative, i.e. either training with VO-A low and then perform tests in condition VO-B low then VO-A low or training with VO-B low and then perform cases VO-A low then VO-B low. The same principle was used in high speed conditions.

It is worth noting that it is of crucial importance that the user keeps the index finger straight and perpendicular to the working plane of the robot throughout the experiments, with the pulp oriented to the left, so that it can make a full and proper contact with the wall. The non-respect of this gesture may

impact the user's perception and the quality of the recorded data. To avoid this, the participants had a sufficient time to familiarize with the interface and practice taping at low and high speeds. Also, data was recorded for each single tap and its exploitability was verified in situ (as for the results given in section 4.2, we checked both visually during the experiments and during data post-processing performed just after each tap that the gesture was performed properly). Each participant was asked to perform taps until we get at least three valid taps (correct speed and absence of contact with the ring before the obstacle).

4.3.2 Results

Between 10 and 15 taps were necessary in each case to obtain three valid taps (one of the subject being unable to perform taps at high speeds, his data were discarded for the analysis).

Figure 14 illustrates the contact speed in each case (the median value appears in red, the box represents the first and third quartiles and the lower and higher bars the extremal values over the 9 trials, i.e. 3 users with 3 taps each). We can observe from these results that our data set is close to the low and high speeds defined in section 4.2 (i.e. 0.2 and 0.4 m/s).

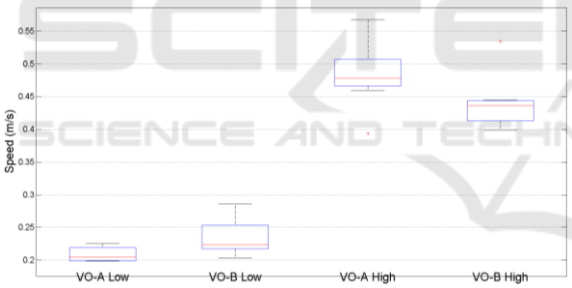

Figure 14: Speed of the ring center at time $t_{r/vo}$.

Figures 15, 16 and 17 illustrate respectively the speed of the ring center when the finger touches it (it should be as low as possible to realistically simulate the wall, which is fixed), the amplitude of the first rebound of the ring against the wall and the highest value of the speed of the ring after contact with the virtual wall (both should be as small as possible).

These results confirm that the behaviour of the interface in conditions VO-A and VO-B is very similar at low speeds. It differs only for high speeds. In this case, the speed of the ring when it encounters the user's finger tends to be closer to zero in condition VO-B (see Figure 15). At least 25% of the samples show positive speed, which means that at contact the ring and the finger were moving in the same direction. This is preferable than having a ring moving against the finger at contact. A clear difference can also be observed if we take into account the rebound d_{max} and the speed $v_{r_{min}}(> to_{f/r})$. Figure 16 shows that conditions VO-A produces a very important rebound compared to VO-B. The same tendency is observed for speeds in Figure 17, the absolute value of the speed in VO-A being much higher than in the VO-B case. The rebound amplitude and speed in VO-B shows a considerable reduction, confirming that conditions VO-B allows a more realistic simulation of a fixed wall, even at high speeds.

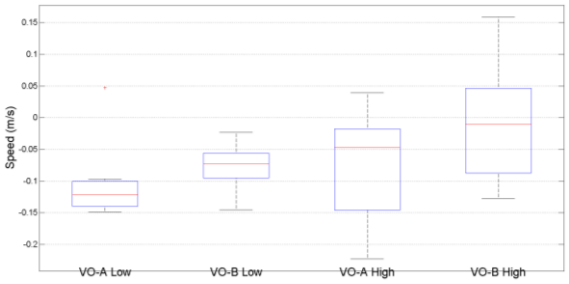

Figure 15: Speed of the ring center at time $to_{f/r}$.

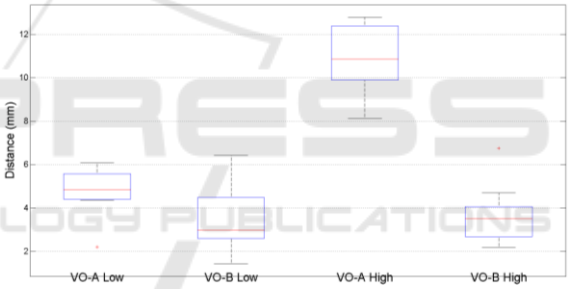

Figure 16: Rebound amplitude d_{max}.

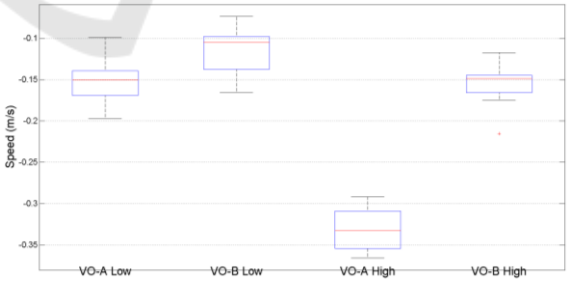

Figure 17: Speed of the ring center at a time $> to_{f/r}$.

Further details on the behaviour of the interface in condition VO-B are given in Table 1. Results show that in average the ring stabilizes in about 3 ms at low speed and 15 ms at high speed, the constraint offset remaining below 3 mm. We can expect that a human operator wouldn't realize these differences when performing a tap (according to (Knorlein et al., 2009)

and (Vogels, 2004), a visuo-haptic delay is imperceptible if it is lower than 45 ms).

Table 1 : Mean and standard deviation for Δsand ε.

mean(std)	Δs (ms)	ε (mm)
Low speed	3.111(2.804)	0.388(0.251)
High speed	14.556(1.424)	2.434(0.357)

The participants were asked to answer three questions after the completion of the tests in each case. Q1 asks if the user perceived the contact before (score 1 or 2), just when (3) or after (4 or 5) the finger's avatar touched the virtual wall. It provides information on the perception of the visuo-haptic delay (ideal result is 3). Q2 asks if at contact the touched wall was perceived as moving to the left (score 1 or 2), being static (3) or moving to the right (4 or 5). It tell us if the user was perceiving the rebound (ideal result is also 3). Finally, Q3 asks if the sensation at contact was felt very natural (1), natural (2), neutral (3), unnatural (4) or very unnatural (5). Results are given in Figure 18 (mean scores for the three participants). They show almost no difference at low speed, as expected. At high speed however, conditions VO-B gives better results. The ring appears static while in VO-A it appears slightly moving. Also, the contact is perceived as being more natural in condition VO-B.

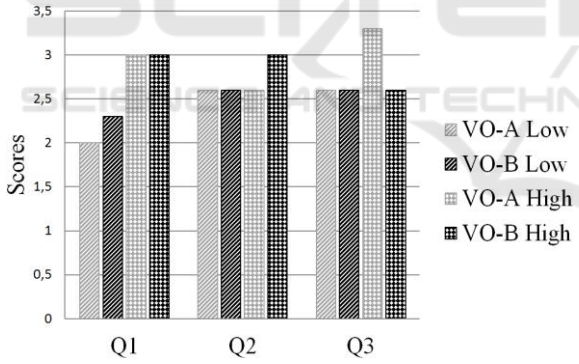

Figure 18: Survey scores.

5 CONCLUSIONS

In this paper, we introduced a new control law intended to improved contact rendering with encounter type haptic displays. The results of our experiments show that this offset transition-based control allows to reduce the speed of the end effector before the user's finger encounters it, as well as its rebound amplitude against the obstacles. As a consequence, the contact is perceived as more natural.

REFERENCES

Achhammer, A., Weber, C., Peer, A., Buss, M. (2010). Improvement of model-mediated teleoperation using a new hybrid environment estimation technique, in: Proc. *IEEE Int. Conf. on Robotics and Automation*, Anchorage, U.S.A., pp. 5358–5363.

Campion, G. (2011) Literature Review. In: Campion, G. (ed) *The Synthesis of Three Dimensional Haptic Textures: Geometry, Control, and Psychophysics*, Springer Series on Touch and Haptic Systems, London, England., Springer-Verlag, pp. 7–44.

Fang, H., Xie, Z., Liu, H. (2009). An exoskeleton master hand for controlling DLR/HIT hand, in: Proc. *IEEE/RSJ Int. Conf. on Intelligent Robots and Systems*, St. Louis, U.S.A., pp. 3703–3708.

Gicquel, P., Bidard, C., Coulon-Lauture, F., Measson, Y., Desbats, P. (2001). Tao: 2000: A generic control architecture for advanced computer aided teleoperation systems, in: *Proc. ANS Int. Topical meeting on Robotics and remote systems*, Seattle, U.S.A.

Gonzalez, F. (2015). *Contributions au développement d'une interface haptique à contacts intermittents (phd thesis)*. Université Pierre et Marie Curie - Paris VI.

Gonzalez, F., Bachta, W., Gosselin, F. (2015a). Smooth transition-based control of encounter-type haptic devices, in: *Proc. IEEE Int. Conf. on Robotics and Automation*, Seattle, U.S.A., pp. 291–297.

Gonzalez, F., Gosselin, F., Bachta, W. (2015b). A 2-D Infrared Instrumentation for Close-Range Finger Position Sensing, *IEEE Trans. on Instrumentation and Measurement*. 64(10), 2708–2719.

Gosselin, F., Bidard, C., Brisset, J. (2005). Design of a High Fidelity Haptic Device for Telesurgery, in: *Proc. IEEE Int. Conf. on Robotics and Automation*, Barcelona, Spain, pp. 205–210.

Hannaford, B. & Okamura, A.M. (2008). Haptics, in: Siciliano, B. & Khatib O. (eds.) *Handbook of Robotics*, Berlin, Germany, Springer, pp. 719–739.

Hayward, V. & Maclean, K.E. (2007) Do it yourself haptics: part I. *IEEE Robotics and Automation Magazine.* 14(4), 88–104.

Knorlein, B., Di Luca, M., Harders, M. (2009). Influence of Visual and Haptic Delays on Stiffness Perception in Augmented Reality, in: *Proc. IEEE Int. Symp. on Mixed and Augmented Reality*, Washington, USA, pp. 49–52.

Martin, S. & Hillier, N. (2009) Characterisation of the Novint Falcon Haptic Device for Application as a Robot Manipulator. In: *Proc. Australasian Conf. on Robotics and Automation*, Sydney, Australia.

McNeely, W.A. (1993). Robotic graphics: a new approach to force feedback for virtual reality, in: *IEEE Virtual Reality Annual Int. Symp.*, Lafayette, Louisiane, pp. 336–341.

McNeely, W.A., Puterbaugh, K.D. & Troy, J.J. (1999). Six Degree-of-freedom Haptic Rendering Using Voxel Sampling, in: *Proc. Annual Conf. on Computer Graphics and Interactive Techniques*, Los Angeles, U.S.A., pp. 401–408.

Nahvi, A., Nelson, D.D., Hollerbach, J.M. & Johnson, D.E. (1998) Haptic manipulation of virtual mechanisms from mechanical CAD designs, in: *Proc. IEEE Int. Conf. on Robotics and Automation*, Leuven, Belgium, pp. 375–380.

Nakagawara, S., Kajimoto, H., Kawakami, N., Tachi, S., Kawabuchi, I., (2005). An Encounter-Type Multi-Fingered Master Hand Using Circuitous Joints, in: *Proc. IEEE Int. Conf. on Robotics and Automation*, Barcelona, Spain, pp. 2667–2672.

Sagardia, M., Hertkorn, K., Hulin, T., Schätzle, S., Wolff, R., Hummel, J., Dodiya, J., Gerndt, A. (2015). VR-OOS: The DLR's virtual reality simulator for telerobotic on-orbit servicing with haptic feedback, in: Proc. *IEEE Aerospace Conf.*, Montana, USA, pp. 1–17.

Samur, E. (2012) *Performance Metrics for Haptic Interfaces*. London, Springer-Verlag.

Tachi, S., Maeda, T., Hirata, R., Hoshino, H. (1994). A construction method of virtual haptic space, in: *Proc. Int. Conf. on Artifitial Reality and Tele-Existence*, Tokyo, Japan.

Vogels, I.M.L.C. (2004). Detection of temporal delays in visual-haptic interfaces. *Human Factors*. (46)1, 118–134.

Yoshikawa, T., Nagura, A. (1997). A touch and force display system for haptic interface, in: *Proc. Int. Conf. on Robotics and Automation*, New Mexico USA, pp. 3018–3024.

Yoshikawa, T., Nagura, A. (1999). A three-dimensional touch/force display system for haptic interface, in: *Proc. IEEE Int. Conf. on Robotics and Automation*, Detroit, USA, pp. 2943–2951.